Developmental Biology 455 (2019) 369–381

Contents lists available at ScienceDirect

Developmental Biology

journal homepage: www.elsevier.com/locate/developmentalbiology

NFAT5/TonEBP controls early acquisition of notochord phenotypic markers, collagen composition, and sonic hedgehog signaling during mouse intervertebral disc embryogenesis

Steven Tessier [a], Vedavathi Madhu [b], Zariel I. Johnson [a], Irving M. Shapiro [a,b], Makarand V. Risbud [a,b,*]

[a] Graduate Program in Cell Biology and Regenerative Medicine, Jefferson College of Life Sciences, Thomas Jefferson University, Philadelphia, PA, USA
[b] Department of Orthopaedic Surgery, Sidney Kimmel Medical College, Thomas Jefferson University, Philadelphia, PA, USA

ARTICLE INFO

Keywords:
Intervertebral disc
Notochord
NFAT5 transcription factor
Sonic hedgehog
Brachyury
Extracellular matrix

ABSTRACT

High osmolarity, bound water, and hydrostatic pressure contribute to notochord mechanics and its morphogenesis into the nucleus pulposus (NP) compartment of the intervertebral disc. Indeed, the osmoadaptive transcription factor, nuclear factor of activated T-cells 5 (NFAT5 aka TonEBP), is robustly expressed by resident cells of the notochord and NP. Nevertheless, the molecular mechanisms that drive notochord osmoregulation and the functions of NFAT5 in disc embryogenesis remain largely unexplored. In this study, we show that deletion of NFAT5 in mice results in delayed vertebral column development and a reduced NP aspect ratio in the caudal spine. This phenotype is associated with lower levels of the T-box transcription factor, Brachyury, delayed expression of notochord phenotypic markers, and decreased collagen II deposition in the perinotochordal sheath and condensing mesenchyme. In addition, NFAT5 mutants showed a stage-dependent dysregulation of sonic hedgehog (Shh) signaling with non-classical expression of Gli1. Generation of mice with notochord-specific deletion of IFT88 (*ShhcreER^{T2};Ift88$^{f/f}$*) supported this mode of Gli1 regulation. Using isolated primary NP cells and bioinformatics approaches, we further show that Ptch1 and Smo expression is controlled by NFAT5 in a cell autonomous manner. Altogether, our results demonstrate that NFAT5 contributes to notochord and disc embryogenesis through its regulation of hallmark notochord phenotypic markers, extracellular matrix, and Shh signaling.

1. Introduction

The notochord is an evolutionarily conserved, rod-like structure encased by a sheath of extracellular matrix. It arises from the node during gastrulation by convergent extension and elongates at the midline, around which the rest of the body plan is oriented (Stemple, 2005). The fundamental roles of the notochord are to coordinate rostro-caudal elongation, provide the embryo with mechanical support, and produce morphogenic factors, such as sonic hedgehog (Shh), which pattern adjacent embryonic tissues (Corallo et al., 2015). To achieve elongation, vertebrate notochord cells exert an outward force against the sheath by increasing their osmotic activity and inflating large lysosome-related cytosolic vacuoles (Adams et al., 1990; Ellis et al., 2013). This restricted osmotic swelling increases the internal pressure of the notochord, forming a stiffened hydrostatic system. As vacuolated notochord cells enlarge and vertebral bodies gradually develop, the physical constraint of the sheath forces notochord cells into regions between developing vertebrae where they settle to form nucleus pulposus (NP) tissue of the intervertebral disc (Choi et al., 2008; Walmsley, 1953). The molecular mechanisms that drive osmoregulation in the notochord and early disc formation, however, remain largely unknown.

In situ RNA hybridization and recent RNA sequencing studies have revealed that the osmoadaptive transcription factor, nuclear factor of activated T-cells 5 (NFAT5 aka TonEBP), is expressed with high specificity in the *Ciona Intestinalis* notochord (José-Edwards et al., 2011; Reeves et al., 2017). Previous studies have also shown that NFAT5 is abundantly expressed in hyperosmotic tissues such as the kidneys and intervertebral discs, where it serves an osmoadaptive role (López-Rodríguez et al., 2004; Tsai et al., 2006). The notochord-derived NP is a hyperosmotic tissue due to an influx of cations drawn by high

* Corresponding author. Department of Orthopaedic Surgery, Thomas Jefferson University, 1025 Walnut Street, Suite 501 College Bldg, Philadelphia, PA, 19107, USA.
E-mail address: makarand.risbud@jefferson.edu (M.V. Risbud).

https://doi.org/10.1016/j.ydbio.2019.07.004
Received 15 February 2019; Received in revised form 12 June 2019; Accepted 9 July 2019
Available online 10 July 2019

concentrations of negatively charged proteoglycans (Ghosh et al., 1975; Ishihara et al., 1997). In NP cells, NFAT5 maintains intracellular osmotic balance by enhancing the expression of key osmoadaptive genes, including tuarine transporter (*Slc6A6*), sodium-*myo*-inositol co-transporter (*Slc5A3*), betaine-GABA transporter (*Slc6A12*), and aldose reductase (*AKR1B1*) (Johnson et al., 2014; Tsai et al., 2006). These genes encode proteins involved in the import and synthesis of organic, non-ionic osmolytes (Burg and Ferraris, 2008), and are of interest with respect to notochord inflation and elongation. Notably, in addition to maintaining intracellular osmotic balance, NFAT5 also controls the extracellular osmotic environment by regulating the expression of key matrix-related genes, including aggrecan, β1,3-glucoronosyltransferase, and collagen II (Hiyama et al., 2009; Tsai et al., 2006; van der Windt et al., 2010). Consequently, NP cell homeostasis is largely maintained by the collective activity of NFAT5-regulated genes.

By employing NFAT5 knockout mice, we have characterized the contribution of NFAT5 in the morphogenesis of notochord into NP. Our results do not support the view that NFAT5 is indispensable for notochord inflation and intervertebral disc development. Instead, we show that lack of NFAT5 results in delayed vertebral column development and changes in the aspect ratio of the caudal NP compartment. This phenotype is associated with lower levels of the T-box transcription factor, Brachyury, delayed expression of notochord phenotypic markers, altered collagen deposition, and dysregulated Shh signaling. *In vitro* experiments using primary NP cells also demonstrate that NFAT5 controls Shh signaling in a cell autonomous manner, lending mechanistic and broader insight into the important role of NFAT5 during notochord and intervertebral disc embryogenesis.

2. Methods

2.1. Mice

C57BL/6 mice heterozygous for deletion of exons 6 and 7 in the *Nfat5* gene were kindly provided by H. Moo Kwan, Ulsan National Institute of Science and Technology (Go et al., 2004). *Nfat5* mice and embryos were genotyped by PCR using primers that span the site of deletion as previously described (Go et al., 2004). $Ift88^{f/f}$ mice were kindly provided by Bradley Yoder, University of Alabama, maintained on a mixed genetic background, and genotyped as previously described (Haycraft et al., 2007). $ShhcreER^{T2}$ mice were obtained from The Jackson Laboratory (Stock # 005623) and crossed with $Ift88^{f/f}$ mice to generate $ShhcreER^{T2}$; $Ift88^{f/+}$ mice. To perform timed pregnancies, mice were paired, allowed to mate overnight, and immediately separated the following morning. Pregnancies were confirmed by copulation plugs and increase in body weight. To generate conditional *Ift88* knockout embryos, pregnant $Ift88^{f/f}$ dams crossed with $ShhcreER^{T2}$; $Ift88^{f/+}$ males were given three consecutive *i.p.* injections of tamoxifen (50 mg/kg, Sigma-Aldrich, St. Louis, MO, USA) dissolved in corn oil (Sigma-Aldrich) starting at E12.5. Time of tamoxifen injection was chosen such that loss of canonical Shh sensing in the notochord would not affect sheath formation and therefore disc development (Choi and Harfe, 2011). Housing, breeding, and embryo collection at E12.5, E13.5, and E17.5 were performed under the guidelines of the Institutional Animal Care and Use Committee of Thomas Jefferson University. Aseptic technique and barrier conditions were used for social housing. Mice were given Lab Diet 5010 Laboratory Autoclavable Rodent *ad libitum*. Experiments were performed with two or more pairs of control and mutant littermates.

2.2. Histological analysis

E17.5 embryos were decalcified in 20% EDTA at 4 °C for 3 days, while E12.5 and E13.5 embryos did not require decalcification. Embryos were fixed in 4% paraformaldehyde (PFA) for 48 h and embedded in paraffin for sectioning in the sagittal plane. 7 μm sections were stained with 1% Safranin-O, 0.05% Fast Green, and 1% Hematoxylin, and then visualized by light microscopy (Axio Imager 2, Carl Zeiss) using 20 × /0,5 EC Plan-Neofluar (Carl Zeiss) or 63 × /1,4 Plan-Apochromat (Carl Zeiss) objectives. Imaging of sections was conducted with the Axiocam 105 color camera (Carl Zeiss) using Zen2™ software (Carl Zeiss). Morphological analysis was performed on eight E12.5, two E13.5, and ten E17.5 null and wild-type embryos. Aspect ratio was measured using ImageJ 1.52a (http://rsb. info.nih.gov/ij/), where the major axis was divided by the minor axis determined by Fit Ellipse measurements. Aspect ratio data were collected from five E17.5 embryos per genotype with three discs per embryo (15 discs).

2.3. Whole mount skeletal preparation

Collected embryos were washed and scalded in hot tap water for 30 s at 65 °C to facilitate removal of skin. Embryos were eviscerated, soft connective tissues were removed, and then embryos were fixed in 4% PFA for 48 h. After fixation, embryos were submerged in Alcian blue (0.03% w/v, 80% EtOH, 20% glacial acetic acid) overnight at room temperature to stain for cartilage. Next, embryos were washed in 70% EtOH followed by 95% EtOH overnight. Alcian blue-stained embryos were then pre-cleared with 1% KOH for 1 h. The KOH solution was replaced with Alizarin red (0.05% w/v in 95% EtOH) solution, stained for 4 h at room temperature, and then overnight at 4 °C to control the rate of staining. To clear embryos, Alizarin red was replaced with a 50% glycerol: 50% (1%) KOH solution and incubated at room temperature until samples were transparent (Rigueur and Lyons, 2014). Morphological analysis was performed on four E17.5 null and three wild-type skeletal preparations.

2.4. TUNEL assay

The *in situ* Cell Death Detection Kit, TMR Red (MilliporeSigma), was used to measure cell death of E12.5 and E17.5 embryonic sections. Slides were heated at 60 °C for 3 h, de-paraffinized, rehydrated through a graded series of ethanol solutions, and permeabilized with boiling citrate-based unmasking solution (pH 6) (Vector Laboratories, H-3301) for 30 min at room temperature. The TUNEL assay was then performed as per manufacturer's protocol. The positive control was generated by treatment with RNase Free DNase I (QIAGEN) (Suppl. Figure 1). Sections were washed with PBS before mounting with ProLong® Gold Antifade Mountant containing DAPI (Thermo Fisher Scientific, P36934), and visualized by fluorescence microscopy (Axio Imager 2, Carl Zeiss) using the 20 × /0,5 EC Plan-Neofluar (Carl Zeiss) objective. The stained sections were imaged using X-Cite® 120Q Excitation Light Source (Excelitas), the AxioCam MRm camera (Carl Zeiss), and Zen2™ software (Carl Zeiss). Staining was performed on four embryonic notochords at E12.5 and five embryos at E17.5 with three representative discs per embryo (15 discs).

2.5. Immunohistochemistry

Sagittal sections were de-paraffinized in histoclear and rehydrated in a series of ethanol solutions (100%–70%). De-paraffinized sections were incubated in boiled citrate-based unmasking solution (Vector Laboratories, H-3301) for 20 min and then cooled to room temperature for 30 min. Next, the sections were incubated for 1 h in the appropriate blocking solution (either 5–10% Normal Goat Serum, 10% Fetal Bovine Serum, or reagent from M.O.M.™ Immunodetection Kit; vector Laboratories, BMK-2202) and subsequently incubated overnight at 4 °C with primary antibody against Brachyury (1:20; R&D, AF2085), CA3 (1:150; Santa Cruz, sc-50715), vimentin (1:200; Cell Signaling, D21H3), β-actin (1:100; Cell Signaling, 13E5), aggrecan (1:50, MilliporeSigma, AB1031), chondroitin sulfate (1:300; Abcam, ab11570), collagen II (1:400, Fitzgerald, 70R-CR008), collagen I (1:100; Abcam, ab34710), Shh (1: 300, Novus, NBP2-22139), Ptch1 (1:200; R&D, MAB41051), Smo (1:50; Abcam, ab72130), Gli1 (1:250; Abcam, ab151796), and

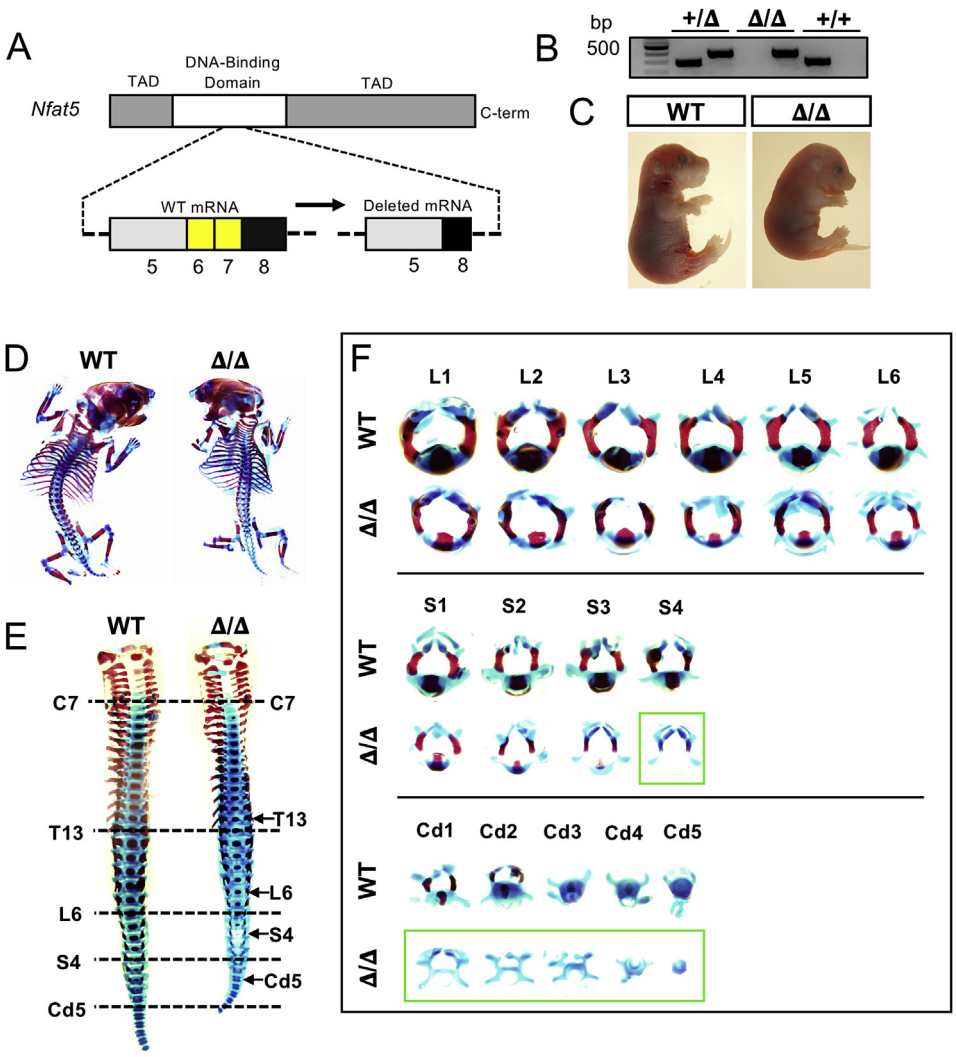

Fig. 1. Deletion of NFAT5 results in delayed development of the vertebral column. (**A**) Diagram showing targeting of exons 6 and 7 of the *Nfat5* gene and resultant mRNA product. (**B**) Agarose gel of PCR-amplified genomic DNA from wild-type (+/+), heterozygous (+/Δ) and null (Δ/Δ) mice. (**C**) Gross comparison of E17.5 embryos showed shorter stature in nulls. (**D**) Whole mount skeletal preparations of NFAT5 mutant embryos at E17.5 stained with alcian blue (cartilage) and alizarin red (bone). (**E**) Comparison of isolated spines showed a shorter vertebral column in mutants than controls. (**F**) Individual lumbar (L1-L6), sacral (S1–S4), and caudal (Cd1–Cd-5) vertebrae of E17.5 mutant mice compared to level-matched controls showed absence of primary ossification centers in the sacrocaudal levels starting at S4 (Green box).

IFT88 (1:250; MilliporeSigma, ABC932). After washing with PBS, sections were incubated for 1 h at room temperature with either Alexa Fluor®-594 or Alexa Fluor®-647 secondary antibodies (1:700, Jackson ImmunoResearch Lab, Inc.). The sections were washed with PBS before mounting with ProLong® Gold Antifade Mountant containing DAPI (Thermo Fisher Scientific, P36934), and visualized by fluorescence microscopy (Axio Imager 2, Carl Zeiss) using the 20 × /0,5 EC Plan-Neofluar (Carl Zeiss) objective. The stained sections were imaged using X-Cite® 120Q Excitation Light Source (Excelitas), the AxioCam MRm camera (Carl Zeiss), and Zen2™ software (Carl Zeiss). Staining of NFAT5 null embryos was performed on four embryos at E12.5, two littermates at E13.5, and five embryos at E17.5 with three representative discs per embryo (n = 15 discs). Staining of *Ift88* conditional knockout embryos was performed on two littermates with four representative discs per embryo (8 discs).

2.6. Digital image analysis

All imaged sections stained by immunohistochemistry were analyzed using ImageJ 1.52a (http://rsb. info.nih.gov/ij/) in the grayscale. The boundaries of the notochord, perinotochordal sheath, and NP were digitally traced using the Freehand Tool. The perinotochordal mesenchyme and condensing mesenchyme were delineated by a rectangular fixed area (300 × 1000 pixels) and circular fixed area (200 × 215 pixels), respectively. These images were then thresholded to create binary images. Designated regions of interest (ROI) were analyzed using the Area Fraction measurement for each section. Area Fraction represents the percentage of positive pixels normalized to ROI, therefore representing protein expression within a given area. Analysis of the notochord, perinotochordal sheath (bilateral average), and perinotochordal mesenchyme (bilateral average) was conducted on four E12.5 embryos per genotype. Analysis of NP tissue was conducted on two E13.5 at four levels per genotype (8 discs) and five E17.5 embryos per genotype with three discs per embryo (15 discs). Fractions of Brachyury-positive nuclei were manually quantified, and fluorescence intensity signals along the line were measured using Zen2™ software (Carl Zeiss). The number of IFT88-positive cells was also manually quantified.

2.7. NP cell isolation and treatment

NP cells were isolated from Sprague Dawley rats (Charles River) as previously described (Risbud et al., 2006). Collection of animal tissues for cell isolation was approved by Thomas Jefferson University IACUC. Cells were maintained in DMEM containing 1g/L glucose with 10% FBS and 1% penicillin-streptomycin, and cultured in a hypoxia work station (Invivo$_2$, Ruskinn, UK) with a mixture of 1% O_2, 5% CO_2 and 94% N_2 to mimic the natural physiological environment of the avascular NP compartment. Either 100/500 nM of SAG (ab142160, abcam) or 5/10 μM of CyA (C-8700, LC Laboratories) was added to medium for 24 h treatment.

2.8. Lentiviral particle production and viral transduction

HEK 293 T cells (ATCC, CRL-3216) were plated in 10 cm plates (5×10^6 cells/plate) in DMEM with 10% heat-inactivated FBS a day before their transfection. Cells were transfected with ShCtr or ShNFAT5 plasmids along with psPAX2 and pMD2.G using Lipofectamine 2000 (MilliporeSigma). Six hours after transfection, medium was replaced with DMEM with 10% heat-inactivated FBS and penicillin-streptomycin. Lentiviral particles were harvested at 48–60 h post-transfection of HEK cells, and precipitated using 7% PEG 6000 (Sigma Aldrich, 81253) solution. NP cells plated in DMEM with 10% heat-inactivated FBS were transduced with lentiviral particles along with 8 μg/ml polybrene (Sigma Aldrich, H9268). Cells were incubated for 16 h and the medium with remaining particle was replaced. Four-five days after transduction, cells were harvested for protein extraction to ensure maximum knockdown efficiency without affecting cell viability. At least 3 independent biological experiments were performed.

2.9. Real-time qRT-PCR

Total RNA was extracted from primary rat NP cells using RNeasy mini columns (Qiagen) and RNase free DNase I (Qiagen). The eluted DNA-free RNA was made into cDNA using EcoDry premix (Clontech). PCR reactions using gene-specific primers (IDT, IA) and SYBR Green master mix (Applied Biosystems) were measured by the Step-One Plus System (Applied Biosystems).

2.10. Protein extraction and Western blotting

Following experimental treatments, notochordal-NP cells were placed on ice and washed with ice-cold PBS. All buffers included 1X-protease inhibitor cocktail (Roche), NaF (4 mM) and Na3VO4 (20 mM), NaCl (150 mM), β-glycerophosphate (50 mM), and DTT (0.2 mM). Protein was resolved on 8–10% SDS-polyacrylamide gels and transferred by electroblotting to activated PVDF membranes (Bio-Rad, CA). Membranes were blocked with 5% non-fat dry milk in TBST (50 mM Tris, pH 7.6, 150 mM NaCl, 0.1% tween 20) and incubated overnight at 4 °C in 3% non-fat dry milk in TBST with anti-Shh (1:1000, Novus, NBP2-22139), Ptch1 (1:500; R&D, MAB41051), Smo (1:1000; Abcam, ab72130), and Gli1 (1:500; Abcam, 151796). Immunolabeling was detected using ECL reagent (Amersham Biosciences). Relative expression levels were determined by quantitative densitometric analysis using 1D image analysis software (ImageQuant, LAS4000).

2.11. Bioinformatics analysis

The nucleotide sequence of the 3 kb proximal promoter of *Shh*, *Ptch1*, and *Smo* genes were identified using the UCSC Table Browser data retrieval tool (Karolchik et al., 2004). Putative TonE consensus sequences were determined using MatInspector (Genomatix Software Suite) with a matrix-similarity threshold of 0.80 and TF family p-value of ~0.05 or below. Analysis of species conservation of putative TonE motifs in rat, mouse, and human was performed by multiz alignment using the UCSC Genome Browser (Kent et al., 2002).

2.12. Statistical analysis

Data is presented as mean ± SD. Differences between genotypes were analyzed using the Student's *t*-test when only two groups presented on graph, or one-way ANOVA with a Sidak's multiple comparison test between groups. All statistical analyses were done using Prism7 (GraphPad Software). $P \leq 0.05$ is considered statistically significant change.

A Key Resources Table (KRT) is included to help identify key materials used in this study.

3. Results

3.1. Loss of NFAT5 delays the development of the vertebral column without inhibiting the formation of intervertebral discs

We investigated intervertebral disc embryogenesis in mice harboring a deletion of exons 6 and 7 of the *Nfat5* gene. Exons 6 and 7 encode a crucial region of the NFAT5 DNA binding domain (Fig. 1A) (Go et al., 2004). Genotypes confirming exon deletion were validated by PCR as described by Go et al. (Fig. 1B) (Go et al., 2004). On gross examination, embryos with homozygous deletions evidenced an overall decrease in body size or were found resorbed due to gestational lethality (Fig. 1C). This decrease in body size was further evidenced by whole mount skeletal preparations stained with alcian blue (cartilage) and alizarin red (bone) (Fig. 1D). Comparison of isolated spines revealed that the thoracic, lumbar, and caudal regions of the vertebral column were notably smaller than controls, likely accounting for the shorter stature of mutants (Fig. 1E). Likewise, individual vertebrae from lumbar (L1-L6), sacral (S1–S4), and caudal (Cd1–Cd-5) levels were undersized compared to level-matched controls (Fig. 1F). While the morphology of the vertebral bodies was generally maintained, the vertebrae showed a marked reduction of primary centers of ossification throughout the lumbar region and complete absence in the sacrocaudal region starting at S4 (Fig. 1F). Since development of the vertebral column progresses from the rostral to the caudal end, this phenotype was consistent with a delay in vertebral body ossification and spinal development. Similar to the axial skeleton, other skeletal structures appeared smaller and the sternum showed lack of ossification. Moreover, lengths of the humerus and femur in mutant embryos were smaller compared to the wild-type littermates (Suppl. Figure 2).

To determine tissue localization of NFAT5 expression during intervertebral disc development, we performed immunohistochemistry on embryos at E12.5, E13.5, and E17.5. Staining revealed that NFAT5 is strongly expressed by cells of the notochord, condensing perinotochordal mesenchyme, early NP, and the hypertrophic zone of the developing vertebral body (Fig. 2A). Mining of deposited RNA-seq data (GSE100934) confirmed that NFAT5 is expressed by notochord cells at E12.5 and NP cells at P0 (Fig. 2B) (Peck et al., 2017). To our surprise, gross histological analysis of the NFAT5 null notochord revealed an intact structure marked by vacuolated notochord cells and strong Safranin-O staining of the perinotochordal sheath (Fig. 2C). However, notochord cell intercalation appeared disorganized in a few embryos, which was evident observing DAPI stained nuclei (Suppl. Figure 3). Further, removal of the notochord at the level of the developing vertebral bodies appeared to be slightly delayed in mutants compared to control mice, in conjunction with a delay in enlargement of prevertebral cells (Fig. 2D). Similar to NFAT5-depleted notochord cells at E12.5, mutant notochordal-NP cells at E13.5 did not show a deficiency in vacuole inflation (Fig. 2D). Likewise, at E17.5, the thoracic and lumbar intervertebral discs developed fully and were populated by vacuolated NP cells (Fig. 2E). These results suggest that while NFAT5 appears to be important for the enlargement of prevertebral cells, it is dispensable for notochord inflation and vacuolation, as well as intervertebral disc formation. Notably, however, E17.5 mutant embryos showed a lower aspect ratio of the caudal NP compartment, while the aspect ratios of the thoracic and lumbar NP were comparable to controls (Fig. 2F). This decrease in aspect ratio was not associated with a decrease in the number of cells per area (Fig. 2G) or increase in cell death as measured by TUNEL assay (Fig. 2H). Indeed, the decrease in aspect ratio of the caudal NP compartment suggests further that NFAT5-deficient embryos experienced developmental delay of the axial skeleton.

3.2. NFAT5 is required for notochord cells to acquire their molecular signature and maintain cytoskeletal integrity

Notochord and developing NP cells have a unique molecular phenotype characterized by expression of several specific markers, including

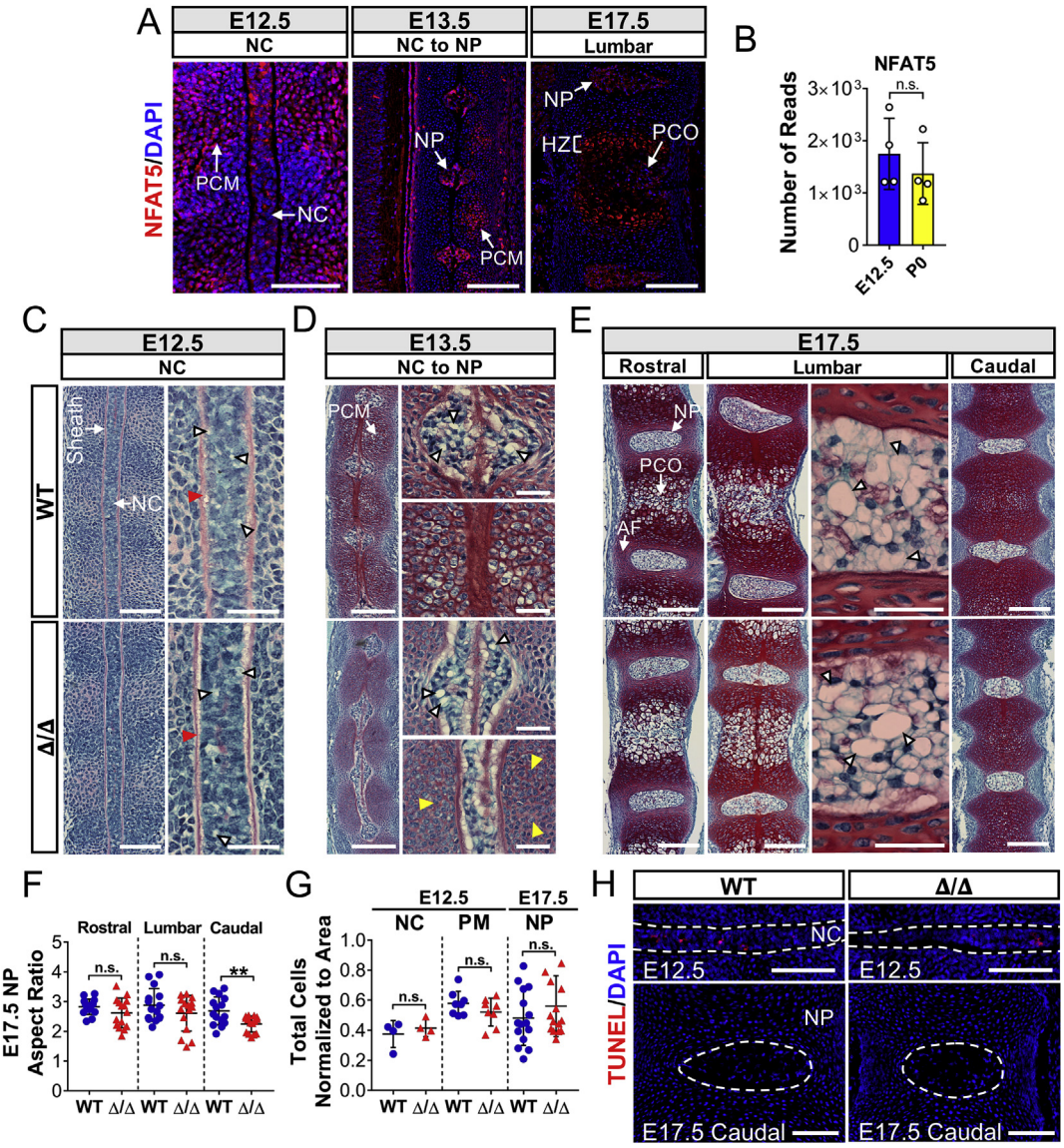

Fig. 2. Loss of NFAT5 results in caudal discs with decreased aspect ratios. (**A**) Localization and expression of NFAT5 at E12.5, E13.5, and E17.5 by immunostaining. Scale bar = 100 μm. PCM: Perinotochordal condensing mesenchyme; NC: Notochord; NP: Nucleus pulposus; PCO: primary center of ossification; HZ: Hypertrophic zone. (**B**) NFAT5 mRNA expression by notochord cells at E12.5 and NP cells at P0 from deposited RNA-seq data (GSE100934). (**C-E**) Sagittal sections of E12.5, E13.5, and E17.5 embryos stained by Safranin-O/Fast Green/Hematoxylin showing notochord morphogenesis into NP at the thoracic, lumbar, and caudal levels. Scale bar = 50 μm. High magnification images showing intact perinotochordal sheath (red arrowheads), delayed enlargement of prevertebral cells at E13.5 (yellow arrowheads), and large intracellular vacuoles at all stages (white arrowheads) (Scale bar = 20 μm). (**F**) Aspect ratios of the caudal but not lumbar and rostral NP of NFAT5 null embryos were significantly smaller than WT embryos. (**G, H**) Changes in aspect ratio were not associated with decreased cell number per area or increased TUNEL positive cells. Scale bar=100 μm. Quantitative measurements represent mean ± SD. n.s. = not significant; **, $p \leq 0.01$.

the T-box transcription factor, Brachyury/T, CA3, and the notochord-enriched intermediate filament, vimentin (Risbud et al., 2015; Risbud and Shapiro, 2011; Sagstad et al., 2011; Silagi et al., 2018a). Analysis of RNA-Seq data (GSE100934) showed that expression of these markers increased from E12.5 to P0, suggesting that their expression coincides with NP cell maturation and/or differentiation (Suppl. Figure 4) (Peck et al., 2017). Interestingly, the expression levels of Brachyury, as measured by quantitative immunohistochemistry, showed a significant decrease at both E12.5 and E17.5 (Fig. 3A, A', C). Importantly, NFAT5 mutants also showed reduced Brachyury nuclear localization, evident from a decrease in the fraction of Brachyury-positive nuclei (Fig. 3B, B', D), as well as out-of-phase fluorescence intensity signals of Brachyury and DAPI (Fig. 3D', D"). In addition, E12.5 mutants showed nearly undetectable levels of carbonic anhydrase 3 (CA3) (Fig. 4A, D) and vimentin (Fig. 4B, E), suggesting delayed notochord maturation. Unlike Brachyury, CA3 and vimentin levels were restored at E17.5, with a small but statistically significant increase in vimentin over wild type embryos (Fig. 4A', B', D, E). These changes in vimentin led us to further examine the cytoskeleton by staining against β-actin, which showed no evidence of altered levels in the notochord, but perturbed and diffused localization at the cortical surface of notochord cells in three of four null embryos (Fig. 4C, F). Similar to vimentin, we also observed that β-actin expression in NP cells was moderately elevated at E17.5 (Fig. 4C', F). Thus, taken altogether, these results reveal that the NFAT5 null notochord exhibits delayed acquisition of its molecular phenotype and shows evidence of a disorganized cytoskeleton.

3.3. Loss of NFAT5 alters deposition of major collagen subtypes during intervertebral disc embryogenesis

We next examined critical extracellular matrix components of the perinotochordal sheath and intervertebral disc in NFAT5 null embryos.

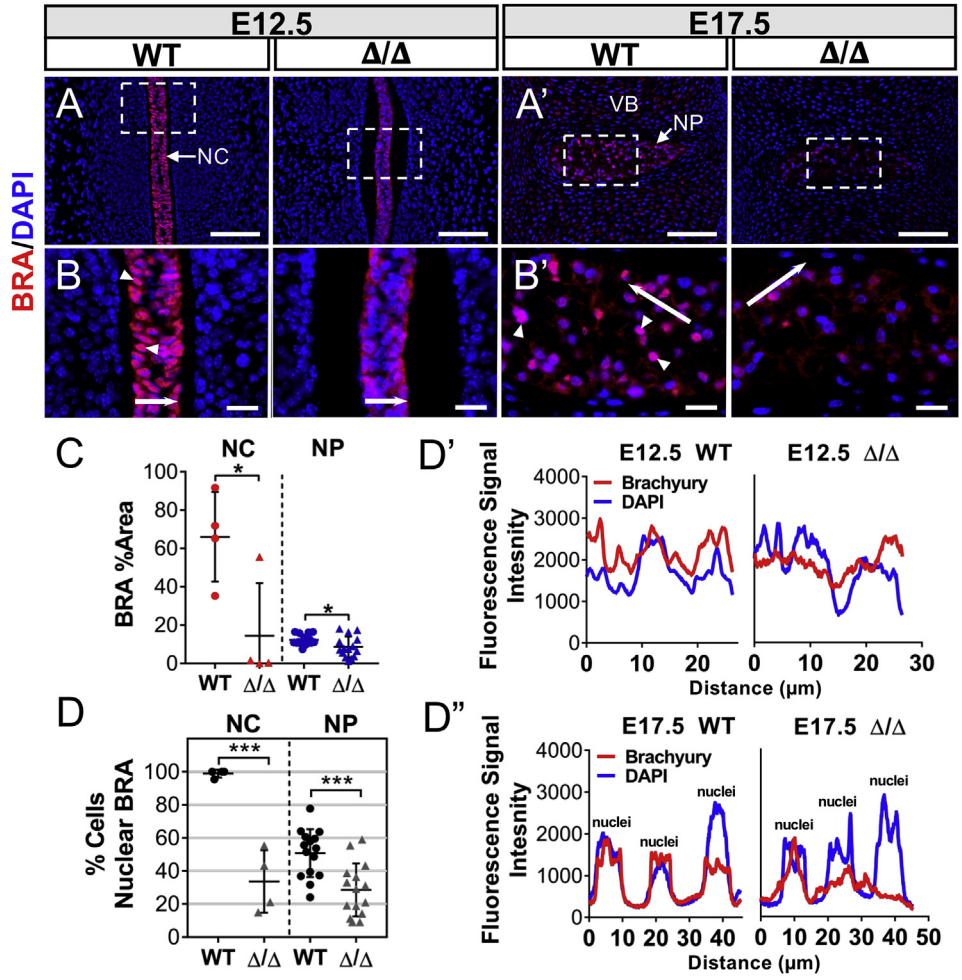

Fig. 3. NFAT5 controls expression and nuclear localization of Brachyury in the notochord and early NP. (**A, A'**) Immunofluorescence staining of Brachyury (BRA) showed decreased expression in both E12.5 notochord (NC) and E17.5 nucleus pulposus (NP). VB: presumptive vertebral body. Scale bar = 100 μm. (**B, B'**) Corresponding high magnification images showed decreased Brachyury nuclear localization (white arrowheads). Scale bar = 20 μm. (**C**) Staining quantified by Area Fraction (% Area) showed lower Brachyury levels in mutants. (**D**) Quantification of Brachyury positive nuclei showed marked reduction in NFAT5 mutants at E12.5 and E17.5 compared to WT embryos. (**D', D"**) Fluorescence intensity along the line in B and B' is plotted in D' for E12.5 and D" for E17.5 embryos, which showed out-of-phase Brachyury and DAPI signals in mutants. Quantitative measurements represent mean ± SD. n.s. = not significant; *, $p \leq 0.05$; ***, $p \leq 0.001$.

Surprisingly, aggrecan (ACAN) and chondroitin sulfate (CS), a glycosaminoglycan that substitutes proteoglycans including aggrecan and versican (Silagi et al., 2018b), showed no differences between null and control embryos at both E12.5 (Fig. 5A, B, E, F) and E17.5 (Fig. 5A', B', E, F), consistent with our Safranin-O staining results. However, collagen II was markedly decreased in the sheath and perinotochordal condensing mesenchyme (PCM) (Fig. 5C, G), while collagen I staining was primarily localized to the sheath and unaffected in E12.5 mutants (Fig. 5D, H). By E17.5, null embryos showed a small increase in levels of both collagen II and I in the NP compartment, with a concomitant decrease in collagen I in the outer annulus fibrosis, possibly reflecting a tissue-specific response to loss of NFAT5 (Fig. 5C', D', G, H). Changes in collagen content were in accord with previous studies using human articular chondrocytes and disc cells, which showed a role of NFAT5 and hyperosmolarity in regulating collagen I and II expression (van der Windt et al., 2010; Wuertz et al., 2007).

3.4. Deletion of NFAT5 results in stage-dependent dysregulation of sonic hedgehog signaling in the notochord and early NP

Sonic hedgehog (Shh) secretion and signaling from the notochord is required for perinotochordal sheath formation and thus patterning of the intervertebral discs (Choi et al., 2012; Choi and Harfe, 2011). Interestingly, the notochord and perinotochordal mesenchyme (PM) showed robust staining of Shh in NFAT5 mutants, demonstrating that NFAT5-deficient notochord cells secreted increased levels of Shh (Fig. 6A, E). On the other hand, patched-1 (Ptch1) expression did not mirror increased Shh levels in both notochord and PM (Fig. 6B, F). Expression of smoothened (Smo) in the notochord of mutants was also similar to wild-type embryos, but with reduced expression in the PM (Fig. 6C, G). Importantly, the downstream effector of Shh signaling glioma-associated oncogene homologue 1 (Gli1) showed elevated expression in notochord and PM, indicating elevated Shh activity (Fig. 6D, H). Interestingly, by E13.5, Shh levels in mutants were reduced and comparable to wild-type controls, with a concomitant decrease in Ptch1 (Fig. 6A', B', E, F). Smo and Gli1 levels were unaffected by this shift (Fig. 6C', D', G, H). By E17.5, Shh and Ptch1 levels in NFAT5 nulls were further reduced, falling significantly below wild type levels (Fig. 6A", B", E, F). Smo, and interestingly Gli1, were unaffected in the NP at this stage despite a precipitous decrease in Shh, suggesting that Gli1 expression was maintained by non-classical mechanisms (Fig. 6C", D", G, H). These results present an interesting model in NFAT5 null embryos wherein the temporal pattern of Shh signaling is exaggerated with induction at E12.5 and suppression by E17.5. To test the hypothesis that Gli1 expression in notochordal-NP cells at E17.5 is maintained in a non-classical fashion, we generated mice with conditional deletion of *Ift88* in notochord cells using *ShhcreER^{T2}* driver (Fig. 6I–K) (Haycraft et al., 2007). Deletion of IFT88 disrupts the formation of functional primary cilia which are critical for canonical Shh sensing (Huangfu et al., 2003). Targeting of *Ift88* in Shh expressing notochord cells did not prevent the formation of intervertebral discs or alter NP cell morphology, as shown by Safranin-O staining (Fig. 6L). Immunostaining and quantification of IFT88-positive NP cells confirmed that IFT88 was knocked out with high efficiency (Fig. 6M, M'). Importantly, Gli1 levels were unaffected in *ShhcreER^{T2}; Ift88$^{f/f}$* embryos (Fig. 6N, N'), suggesting that primary cilia-mediated Shh signaling was not required for maintenance of Gli1 expression in NP cells at this stage of development.

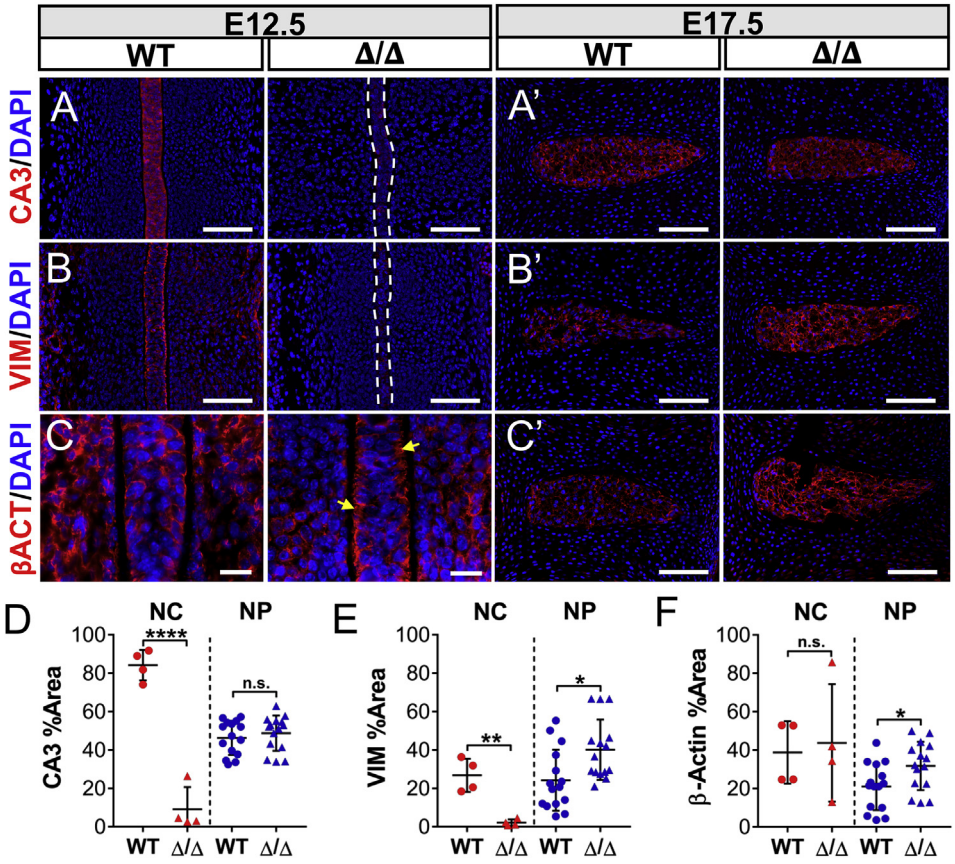

Fig. 4. The NFAT5 null notochord exhibits delayed acquisition of its molecular phenotype and shows evidence of a disorganized cytoskeleton. (**A, A'**) Deletion of NFAT5 significantly reduced notochordal expression levels of carbonic anhydrase 3 (CA3), whereas expression was restored in the NP at E17.5. (**B, B'**) Mutant notochord showed nearly undetectable expression levels of vimentin (VIM), with increased levels in the NP at E17.5. Scale bar = 100 μm (**C**) High magnification images show reduced *β*-actin localization to the submembranous cortex in null notochord cells (yellow arrows). Scale bar = 20 μm. (C, C') There were no changes in *β*-actin expression at E12.5 between genotypes, however, E17.5 embryos showed moderately increased levels. Scale bar = 100 μm. Staining against CA3 (**D**), vimentin (**E**), and *β*-actin (**F**) was quantified by Area Fraction (% Area). Quantitative measurements represent mean ± SD. n.s. = not significant; *, $p \leq 0.05$; **, $p \leq 0.01$; ****, $p \leq 0.0001$.

3.5. NFAT5-mediated regulation of sonic hedgehog signaling is cell autonomous in NP cells

We aimed to establish a mechanistic relationship between NFAT5 and Shh signaling. In particular, we investigated whether NFAT5 controlled Shh or whether fluctuations in Shh were compensatory due to loss of NFAT5. To this effect, we stably knocked down NFAT5 in primary NP cells and measured expression of Shh and its signaling components. Knockdown resulted in increased Shh mRNA levels, whereas a robust decrease in Ptch1 and Smo transcripts were seen without any concomitant change in Gli1 (Fig. 7A). Western blot analysis confirmed a significant decrease in protein levels of Ptch1 and to a smaller extent Smo without changes in Gli1. In contrast to Shh transcript, however, Shh protein levels remained unaffected in NFAT5 knockdown cells, suggesting the possibility of further translational or post-translational regulation (Fig. 7B). These results also raised a possibility that NFAT5 may control expression of Ptch1 and Smo independent of Shh. It is known that NFAT5 transactivates downstream targets by binding to tonicity-response elements (TonE) in gene promoters; therefore, we investigated whether *Shh*, *Ptch1,* and *Smo* contain potential TonE sites within their proximal promoters. Analysis of 3 kb proximal promoter sequences using MatInspector (Genomatix Software Suite) identified putative TonE binding sites in the rat (4 sites) and mouse (3 sites) *Ptch1* promoter. Multiz alignment showed that two of these TonE binding sites were highly conserved among rat, mouse, and human, suggesting that these sites are physiologically relevant (Fig. 7C). Analysis also identified four putative TonE binding sites in the rat and mouse and six sites in human *Smo* promoter, with one site conserved between rat and mouse (Fig. 7C). Interestingly, however, we did not find predicted TonE binding sites in the *Shh* promoter, suggesting the possibility that its transcriptional induction in NFAT5 knocked down cells was due to a compensatory response to reduced Ptch1 and Smo levels. To investigate if Shh signaling modulates NFAT5 expression, we measured NFAT5 mRNA and protein levels in NP cells following treatment with smoothened agonist, SAG, and smoothened inhibitor, cyclopamine (CyA). NFAT5 mRNA and protein levels were refractory to either treatment whereas Gli1 mRNA was responsive to both treatments (Fig. 7D-F'). Altogether, these results suggest that NFAT5 controls Shh signaling by functioning as a positive regulator of Ptch1 and possibly Smo expression in an NP cell autonomous manner (see Fig. 8).

4. Discussion

NFAT5 is robustly expressed by resident cells of the *Ciona* notochord and, as shown here, by cells of the mouse notochord, and plays a critical role in maintaining osmoadaptation and matrix homeostasis in NP cells (Johnson et al., 2014; José-Edwards et al., 2011; Reeves et al., 2017). However, there are no studies that have directly addressed the role of NFAT5 in notochord biology and its morphogenesis into NP or in the formation of the intervertebral discs. Using genetic mouse models, *in vitro,* and bioinformatics approaches, we provide the first insights into the contribution of NFAT5 during these early morphogenic events.

Our analysis suggests that NFAT5 deletion results in developmental delay of the vertebral column. First, at E17.5, mutant spines were shorter in length with undersized vertebral bodies and a significant delay in the formation of primary ossification centers, most noticeably in the sacrocaudal region. Since the caudal-most vertebral column is the last to develop during spinal skeletogenesis, it is not unreasonable to assume that a delay in its development would be more apparent in the caudal region. This idea is further supported by the observation that null embryos showed decreased aspect ratios of the NP compartment at the caudal levels, but not at the thoracic and lumbar levels. Second, at E13.5, we observed what appeared to be a delay in the enlargement or maturation of prevertebral cells, lending the possibility that NFAT5 plays an important role in chondrocyte development. A delay in chondrocyte development might also explain why the condensing mesenchyme of

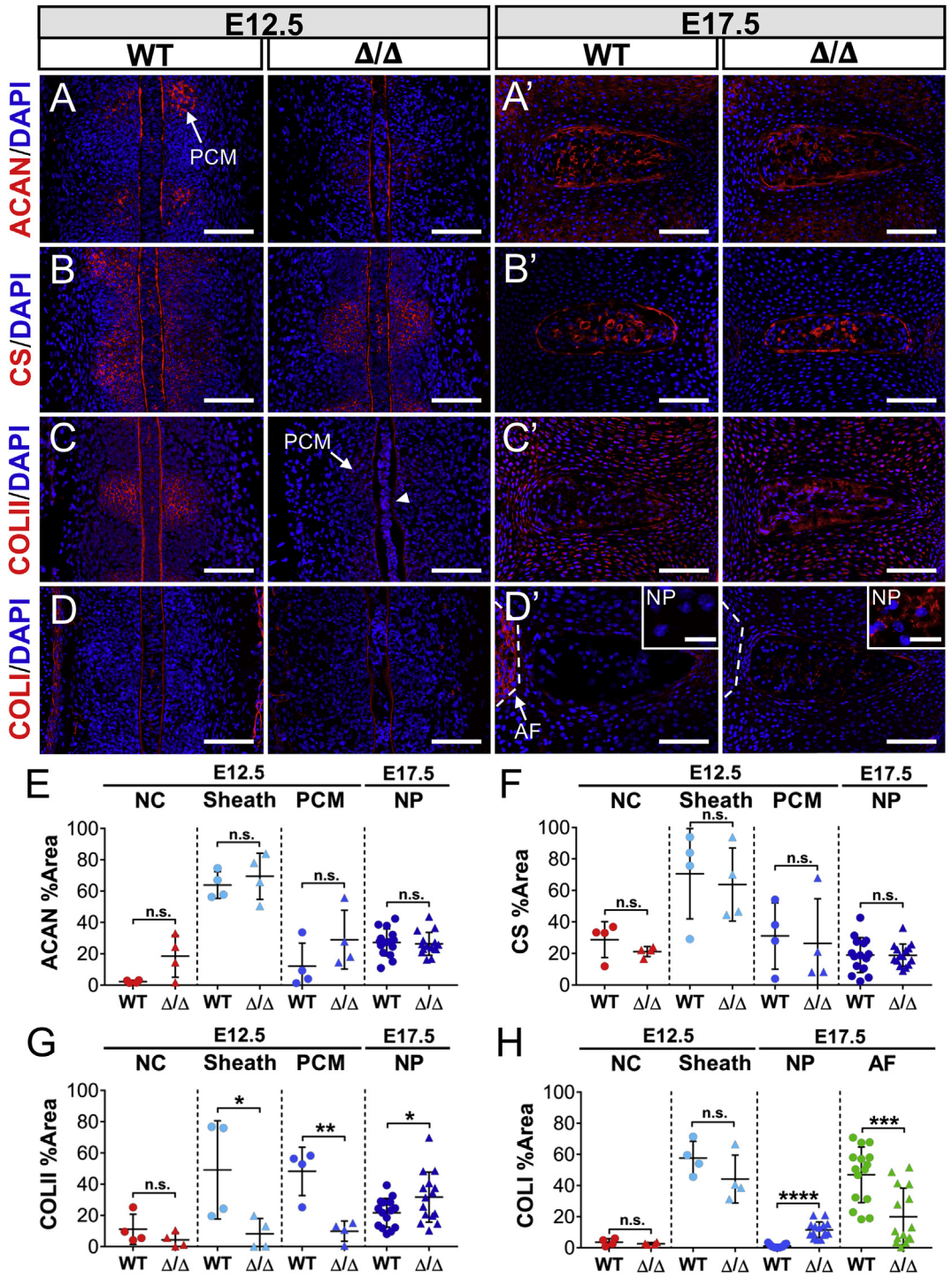

Fig. 5. NFAT5 mutants show altered levels of collagen I and II. Immunofluorescence staining of (**A, A'**) aggrecan (ACAN) and (**B, B'**) chondroitin sulfate (CS) showed no discernible differences between genotypes at both E12.5 and E17.5. Decreased levels of (**C**) collagen II (COLII) in the sheath (arrowhead) and perinotochordal condensing mesenchyme (PCM) were observed at E12.5. (**C'**) At E17.5, collagen II levels were restored and moderately increased in the NP. (**D, D'**) While collagen I (COLI) was unaffected by NFAT5 deletion at E12.5, expression levels were increased in the NP, with lower levels in the outer AF. Scale bar = 100 μm. Inset scale bar = 20 μm. (**E-H**) Immunofluorescence staining of the notochord, perinotochordal sheath, PCM, and NP were quantified by Area Fraction (% Area). Quantitative measurements represent mean ± SD. n.s. = not significant; *, $p \leq 0.05$; **, $p \leq 0.01$; ***, $p \leq 0.001$; ****, $p \leq 0.0001$.

E12.5 embryos showed lower levels of collagen II. Third, the notochord phenotypic markers Brachyury, carbonic anhydrase 3 (CA3), and vimentin, all of which were seen to be associated with notochord cell maturation and NP cell differentiation, were under-expressed at E12.5. Lastly, as Shh is most strongly expressed by notochord cells at early stages of development, increased Shh levels at E12.5 in both NFAT5 null notochord and adjacent mesenchyme is consistent with a delay in development. Altogether, these results suggest that NFAT5 is required for early notochord cell maturation and acquisition of the notochord molecular signature, and for controlling the temporal progression of vertebral column development.

It is plausible that the observed caudal abnormalities were in part due to compromised Brachyury expression and activity. Indeed, it is known that adult mice heterozygous for Brachyury show a short-tail

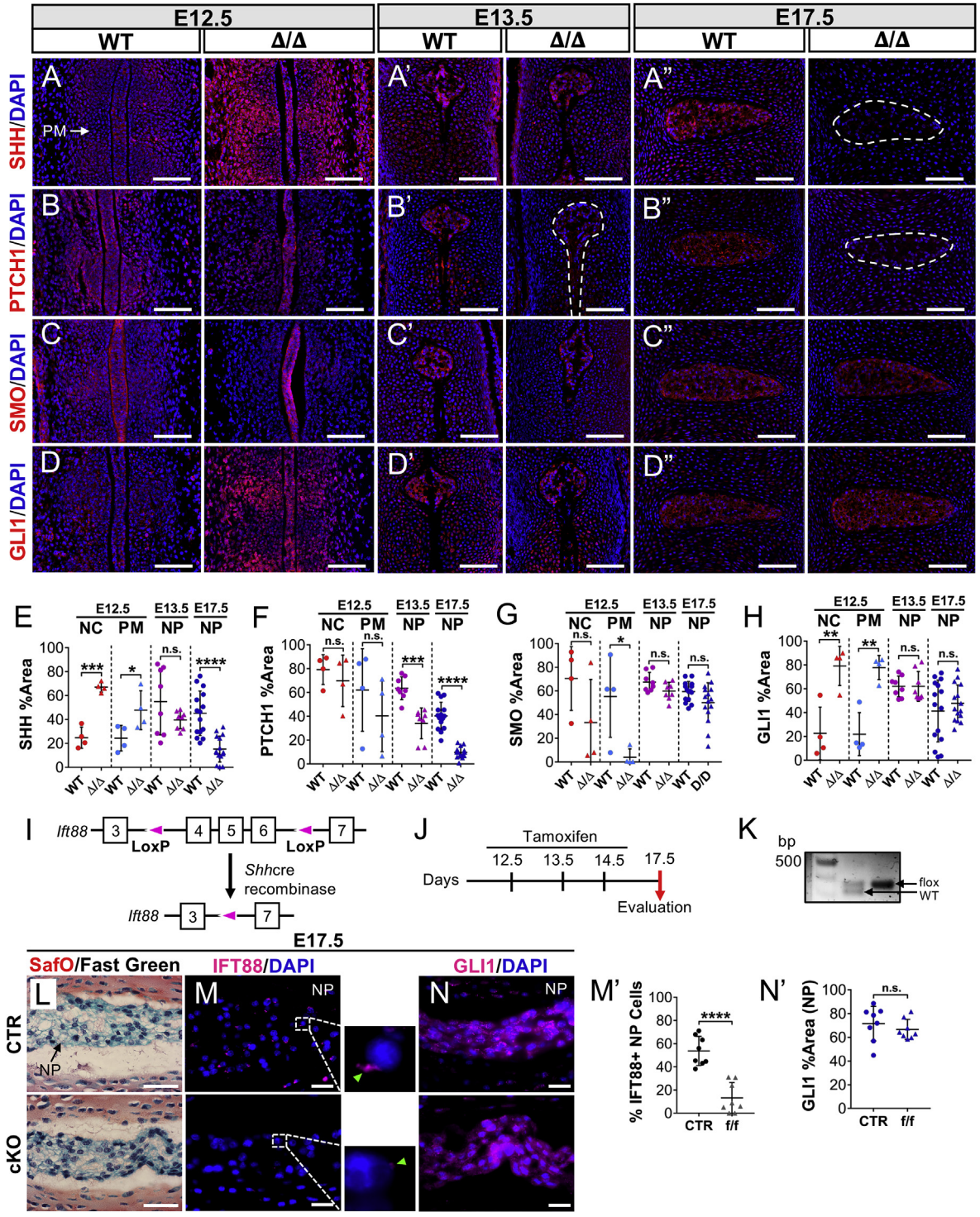

Fig. 6. NFAT5 null embryos show stage-dependent dysregulation of sonic hedgehog signaling involving nonclassical expression of Gli1. (**A**) Sonic hedgehog (SHH) in NFAT5 mutants showed elevated expression levels in both the notochord and perinotochordal mesenchyme (PM) at E12.5. (**A', A"**) Shh Levels in early NP were similar to wild-type at E13.5 and then markedly reduced at E17.5. (**B**) Patched-1 (PTCH1) levels in mutants did not mirror elevated Shh in the notochord and PM. (**B', B"**) Minimal Ptch1 expression was observed in the mutant NP at E13.5 and E17.5. (**C**) NFAT5 nulls showed normal levels of smoothened (SMO) in the notochord with decreased levels in the PM. (**C', C"**) At E13.5 and E17.5, no differences were seen between groups. (**D, D'**) In mutants, glioma-associated oncogene homologue 1 (GLI1) levels increased in the notochord and PM at E12.5, and mirrored Shh levels in the early NP at E13.5. (**D"**) Gli1 levels were refractory to NFAT5 deletion at E17.5. Scale bar = 100 μm. (**E-H**) Staining of the notochord, PM, and NP was quantified by Area Fraction (% Area). (**I**) Schematic representing the generation of *Ift88* null allele in *Shh* expressing cells. (**J**) Timeline showing tamoxifen injection strategy to conditionally knockout *Ift88* without disrupting disc development. (**K**) Agarose gel of PCR-amplified genomic DNA confirming *Ift88* floxed alleles. (**L**) Representative images of sagittal sections of intervertebral discs from E17.5 $ShhcreER^{T2}$;$Ift88^{f/f}$ (cKO) animals stained by Safranin-O/Fast Green/Hematoxylin compared to controls. (**M, M'**) Immunostaining and quantification of IFT88-positive NP cells confirmed that IFT88 was knocked out with high efficiency. (**N, N'**) Gli1 levels were unaffected in $ShhcreER^{T2}$; $Ift88^{f/f}$ embryos. Sale bars=20 μm. Quantitative measurements represent mean ± SD. n.s.=not significant; *, $p \leq 0.05$; **, $p \leq 0.01$; ***, $p \leq 0.001$; ****, $p \leq 0.0001$.

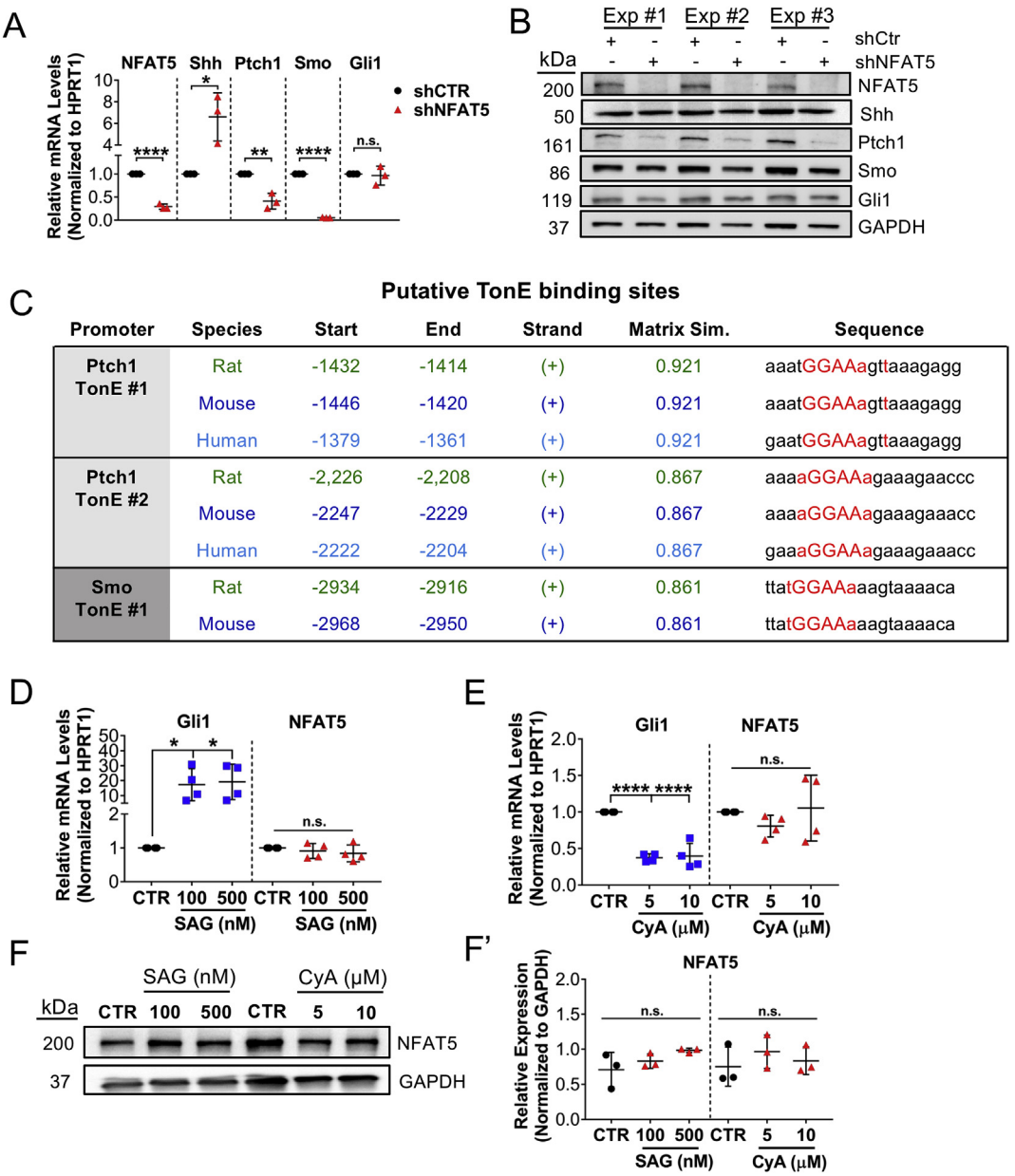

Fig. 7. NFAT5-mediated regulation of Shh signaling is cell-autonomous in NP cells. (**A**) mRNA levels of *Nfat5*, *Ptch1*, and *Smo* were significantly suppressed in NP cells transduced with *Nfat5* shRNA (shNFAT5) compared to control shRNA (shCtr). mRNA levels of *Shh* were markedly increased in shNFAT5 cells, whereas *Gli1* mRNA levels were not affected (n = 3). (**B**) Western blot of three independent biological experiments showed significantly decreased protein levels of Ptch1 and to a smaller extent Smo with no change in Gli1 following *Nfat5* knockdown. In contrast to *Shh* transcript, Shh protein levels remained unaffected in knockdown cells. (**C**) Predicted TonE binding sites identified by MatInspector (Genomatix Software Suite) in the proximal promoters of *Ptch1* and *Smo* in rat, mouse, and human showed high conservation. (**E**) Activation of canonical Shh signaling in NP cells with Smo agonist (SAG) induced *Gli1* mRNA but not *Nfat5* mRNA levels (n = 4). (**F**) Treatment with the Smo inhibitor cyclopamine (CyA) reduced levels of *Gli1* mRNA but not *Nfat5* mRNA (n = 4). Protein levels of NFAT5 measured by Western blot (**G**) and corresponding densitometry from three independent biological experiments (**G'**) showed no effect on expression by both SAG and CyA treatment (n = 3). In G, one representative Western blot is shown. Quantitative measurements represent mean ± SD. n.s. = not significant; *, $p \leq 0.05$; **, $p \leq 0.01$; ***, $p \leq 0.001$; ****, $p \leq 0.0001$.

phenotype—hence the ancient Greek name "*Brachy* (short) *-ury* (tail)", and several examples of sacral/caudal defects associated with dysregulated Brachyury have been examined (Chiba et al., 2009; Ghebranious et al., 2008; Korzh and Grunwald, 2001; Pennimpede et al., 2012; Postma et al., 2014; Stott et al., 1993). While our data suggests that NFAT5 maintains Brachyury expression in both the mouse notochord and newly formed NP, José-Edwards and colleagues have also demonstrated that notochord expression of the *Ciona* NFAT5 ortholog is markedly decreased in a large percentage of Brachyury null embryos (José-Edwards et al., 2011). These results lend the possibility that a bidirectional regulatory circuit exists between NFAT5 and Brachyury. Interestingly, it has been shown that attenuation of Brachyury by overexpression of dominant-negative NFAT5 can be rescued by stabilizing β-catenin (Adachi et al., 2012), suggesting that this relationship might be mediated by canonical Wnt signaling.

In addition to changes in notochord phenotypic marker expression, NFAT5 null embryos showed a stage-dependent dysregulation of Shh signaling, in which Shh levels were significantly elevated at E12.5 and decreased by E17.5. Shh signaling is required for the formation of the matrix-rich perinotochordal sheath, which is necessary for containing

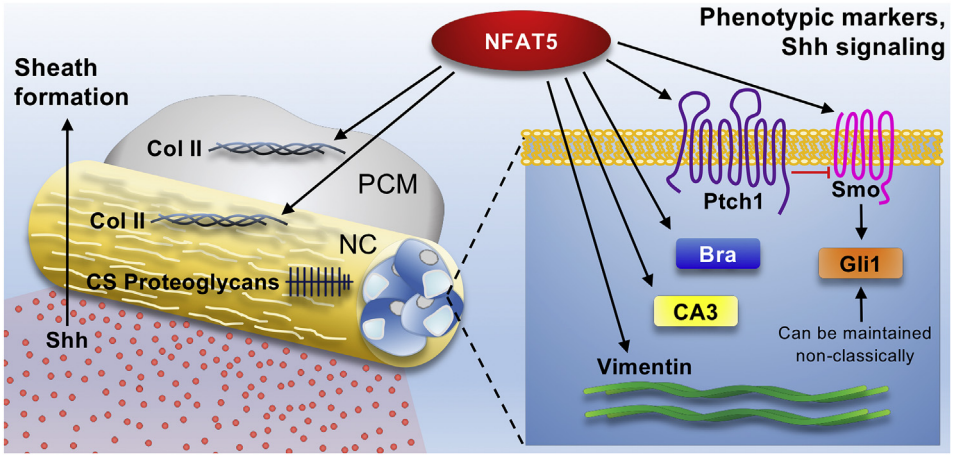

Fig. 8. Model showing the role of NFAT5 in notochord morphogenesis. NFAT5 regulates expression levels of notochordal phenotypic markers Brachyury, CA3, and vimentin, while also controlling Shh signaling in notochord cells and collagen II deposition in the perinotochordal sheath and condensing mesenchyme. NC: Notochord; PCM: Perinotochordal condensing mesenchyme.

notochord cells during early disc patterning, but not for maintaining the embryonic nuclei pulposi once they are formed (Choi and Harfe, 2011). It is therefore possible that Shh was elevated in NFAT5 mutants at E12.5 to ensure that the collagen II-depleted sheath was formed sufficiently for disc patterning to occur. Indeed, Shh is most strongly expressed by notochord cells at early stages of mouse development and fall precipitously by 88 fold from E12.5 to P0 (Peck et al., 2017). Notably, while we observed elevated Shh and Gli1 levels at E12.5, Ptch1 levels did not mirror this increase, and were later decreased at E13.5 and E17.5. These results, along with our *in vitro* findings that Ptch1 transcript and protein levels were suppressed by knockdown of NFAT5, raises an intriguing possibility that NFAT5 regulates Ptch1 expression independent of Shh. In corroboration of this hypothesis, analysis of the proximal Ptch1 promoter revealed two highly conserved TonE binding sites, suggesting that Ptch1 is a target of NFAT5. Interestingly, analysis of the Smo promoter also predicted a conserved TonE binding site, which might explain why Smo levels showed a downward trend *in vivo* and decreased with NFAT5 knockdown *in vitro*. Another notable observation in mutant embryos was that Gli1 levels did not decrease with declining Shh and Ptch1 levels at E17.5, consistent with our observation that Gli1 transcript and protein levels were refractory to NFAT5 knockdown *in vitro*. Furthermore, notochord-specific conditional deletion of IFT88, an intraflagellar transport protein which maintains functional primary cilia and thus canonical Shh sensing (Huangfu et al., 2003), did not decrease Gli1 levels at E17.5. These results clearly suggest that Gli1 expression by embryonic NP cells can be maintained by non-classical mechanisms. Indeed, non-classical activation of Gli1 can occur through numerous pathways, including TGF-β and Notch signaling, which are active in embryonic and post-natal NP cells (Aberger et al., 2012; Chan et al., 2014; Hiyama et al., 2011; Tran et al., 2010).

While NFAT5 null embryos showed interesting phenotypic and molecular changes, loss of NFAT5 had modest effects on the formation and morphology of the notochord and intervertebral discs, implying that NFAT5 was dispensable for notochord inflation and notochordal-NP cell vacuolation. This result is quite surprising because NFAT5 is the only known tonicity-responsive transcription factor in mammals (López-Rodríguez et al., 2001). Second, notochord inflation is widely understood to utilize transmembrane channels, transporters, and pumps to build an osmotic gradient and draw osmotically obliged water into the notochord (Adams et al., 1990; Deng et al., 2013; Reeves et al., 2017). Accordingly, while NFAT5 is primarily involved in regulating organic, non-ionic osmolytes, perhaps ionic gradients independent of NFAT5 activity are of greater importance in driving notochord inflation and notochordal-NP cell vacuolation. In addition, because NP cells begin to deposit negatively-charged glycosaminoglycan-rich matrix during the later stages of disc development, it is possible that the osmoprotective role of NFAT5 is not apparent until greater amounts of matrix are accumulated. Consistent with this speculation, NFAT5-deficient NP cells at E17.5 upregulated their production of vimentin and β-actin, perhaps to resist the osmotic challenge presented by continued extracellular matrix deposition. Yet still, it is possible that osmoprotection is more important in *Ciona*, given that, unlike vertebrates, the *Ciona* notochord forms extracellular lumens of water-imbibing matrix (Lu et al., 2018). It is also important to note that the modest phenotype in mutants is unlikely due to compensation of NFAT5 function by other members of the NFAT family, NFAT1-4. While these family members can regulate expression of NFAT5 target genes associated with inflammatory responses, they cannot compensate osmoadaptive functions that require binding to TonE sites, where cooperative binding with AP1 and p65 is not involved (Johnson et al., 2017, 2016; Lopez-Rodríguez et al., 1999; Macián et al., 2001; Miyakawa et al., 1999; Stroud et al., 2002).

In summary, our results do not support the view that NFAT5 is indispensable for notochord inflation and intervertebral disc development in vertebrates. Instead, we reveal that deletion of NFAT5 results in delayed vertebral column development and delayed expression of notochord phenotypic markers. Further, we show that NFAT5 controls Shh signaling by regulation of Ptch1 and Smo, and that Gli1 expression in embryonic NP cells can be maintained despite loss of Shh signaling. For the first time, these results thus offer mechanistic and broader insight into the important role of NFAT5 during notochord and intervertebral disc embryogenesis.

Author contributions

Study design: MVR and ST. Study conduct: MVR, IMS. Data collection: ST, VM, ZIJ. Data analysis: ST. Data interpretation: MVR, ST. Drafting manuscript: MVR, ST. Revising manuscript content: MVR, IMS, ST, VM, ZIJ. Approving final version of manuscript: MVR, IMS, ST, VM, ZIJ. MVR takes responsibility for the integrity of the data analysis.

Funding

This work was supported by National Institute of Arthritis and Musculoskeletal and Skin Diseases of the National Institutes of Health under [grant numbers R01AR064733, R01AR055655, R01AR074813, T32AR052273].

Declarations of interest

None.

Acknowledgements

We kindly thank Emanuel Novais for performing tamoxifen injections and Elizabeth Silagi for conducting the bioinformatics analysis.

Appendix A. Supplementary data

Supplementary data to this article can be found online at https://doi.org/10.1016/j.ydbio.2019.07.004.

References

Aberger, F., Kern, D., Greil, R., Hartmann, T.N., 2012. Canonical and noncanonical Hedgehog/GLI signaling in hematological malignancies. Vitam. Horm. 88, 25–54. https://doi.org/10.1016/B978-0-12-394622-5.00002-X.

Adachi, A., Takahashi, T., Ogata, T., Imoto-Tsubakimoto, H., Nakanishi, N., Ueyama, T., Matsubara, H., 2012. NFAT5 regulates the canonical Wnt pathway and is required for cardiomyogenic differentiation. Biochem. Biophys. Res. Commun. 426, 317–323. https://doi.org/10.1016/j.bbrc.2012.08.069.

Adams, D.S., Keller, R., Koehl, M.A., 1990. The mechanics of notochord elongation, straightening and stiffening in the embryo of Xenopus laevis. Development 110, 115–130.

Burg, M.B., Ferraris, J.D., 2008. Intracellular organic osmolytes: function and regulation. J. Biol. Chem. 283, 7309–7313. https://doi.org/10.1074/jbc.R700042200.

Chan, W.C.W., Au, T.Y.K., Tam, V., Cheah, K.S.E., Chan, D., 2014. Coming together is a beginning: the making of an intervertebral disc. Birth Defects Res C Embryo Today 102, 83–100. https://doi.org/10.1002/bdrc.21061.

Chiba, S., Jiang, D., Satoh, N., Smith, W.C., 2009. Brachyury null mutant-induced defects in juvenile ascidian endodermal organs. Development 136, 35–39. https://doi.org/10.1242/dev.030981.

Choi, K.-S., Cohn, M.J., Harfe, B.D., 2008. Identification of nucleus pulposus precursor cells and notochordal remnants in the mouse: implications for disk degeneration and chordoma formation. Dev. Dynam. 237, 3953–3958. https://doi.org/10.1002/dvdy.21805.

Choi, K.-S., Harfe, B.D., 2011. Hedgehog signaling is required for formation of the notochord sheath and patterning of nuclei pulposi within the intervertebral discs. Proc. Natl. Acad. Sci. U. S. A. 108, 9484–9489. https://doi.org/10.1073/pnas.1007566108.

Choi, K.-S., Lee, C., Harfe, B.D., 2012. Sonic hedgehog in the notochord is sufficient for patterning of the intervertebral discs. Mech. Dev. 129, 255–262. https://doi.org/10.1016/j.mod.2012.07.003.

Corallo, D., Trapani, V., Bonaldo, P., 2015. The notochord: structure and functions. Cell. Mol. Life Sci. 72, 2989–3008. https://doi.org/10.1007/s00018-015-1897-z.

Deng, W., Nies, F., Feuer, A., Bocina, I., Oliver, D., Jiang, D., 2013. Anion translocation through an Slc26 transporter mediates lumen expansion during tubulogenesis. Proc. Natl. Acad. Sci. U. S. A. 110, 14972–14977. https://doi.org/10.1073/pnas.1220884110.

Ellis, K., Bagwell, J., Bagnat, M., 2013. Notochord vacuoles are lysosome-related organelles that function in axis and spine morphogenesis. J. Cell Biol. 200, 667–679. https://doi.org/10.1083/jcb.201212095.

Ghebranious, N., Blank, R.D., Raggio, C.L., Staubli, J., McPherson, E., Ivacic, L., Rasmussen, K., Jacobsen, F.S., Faciszewski, T., Burmester, J.K., Pauli, R.M., Boachie-Adjei, O., Glurich, I., Giampietro, P.F., 2008. A missense T (Brachyury) mutation contributes to vertebral malformations. J. Bone Miner. Res. 23, 1576–1583. https://doi.org/10.1359/jbmr.080503.

Ghosh, P., Taylor, T.K., Horsburgh, B.A., 1975. The composition and protein metabolism in the immature rabbit intervertebral disc. Cell Tissue Res. 163, 223–238. https://doi.org/10.1007/BF00221729.

Go, W.Y., Liu, X., Roti, M.A., Liu, F., Ho, S.N., 2004. NFAT5/TonEBP mutant mice define osmotic stress as a critical feature of the lymphoid microenvironment. Proc. Natl. Acad. Sci. U. S. A. 101, 10673–10678. https://doi.org/10.1073/pnas.0403139101.

Haycraft, C.J., Zhang, Q., Song, B., Jackson, W.S., Detloff, P.J., Serra, R., Yoder, B.K., 2007. Intraflagellar transport is essential for endochondral bone formation. Development 134, 307–316. https://doi.org/10.1242/dev.02732.

Hiyama, A., Gajghate, S., Sakai, D., Mochida, J., Shapiro, I.M., Risbud, M.V., 2009. Activation of TonEBP by calcium controls {beta}1,3-glucuronosyltransferase-I expression, a key regulator of glycosaminoglycan synthesis in cells of the intervertebral disc. J. Biol. Chem. 284, 9824–9834. https://doi.org/10.1074/jbc.M807081200.

Hiyama, A., Skubutyte, R., Markova, D., Anderson, D.G., Yadla, S., Sakai, D., Mochida, J., Albert, T.J., Shapiro, I.M., Risbud, M.V., 2011. Hypoxia activates the notch signaling pathway in cells of the intervertebral disc: implications in degenerative disc disease. Arthritis Rheum. 63, 1355–1364. https://doi.org/10.1002/art.30246.

Huangfu, D., Liu, A., Rakeman, A.S., Murcia, N.S., Niswander, L., Anderson, K.V., 2003. Hedgehog signalling in the mouse requires intraflagellar transport proteins. Nature 426, 83–87. https://doi.org/10.1038/nature02061.

Ishihara, H., Warensjo, K., Roberts, S., Urban, J.P., 1997. Proteoglycan synthesis in the intervertebral disk nucleus: the role of extracellular osmolality. Am. J. Physiol. 272, C1499–C1506. https://doi.org/10.1152/ajpcell.1997.272.5.C1499.

Johnson, Z.I., Doolittle, A.C., Snuggs, J.W., Shapiro, I.M., Le Maitre, C.L., Risbud, M.V., 2017. TNF-α promotes nuclear enrichment of the transcription factor TonEBP/NFAT5 to selectively control inflammatory but not osmoregulatory responses in nucleus pulposus cells. J. Biol. Chem. 292, 17561–17575. https://doi.org/10.1074/jbc.M117.790378.

Johnson, Z.I., Shapiro, I.M., Risbud, M.V., 2014. Extracellular osmolarity regulates matrix homeostasis in the intervertebral disc and articular cartilage: evolving role of TonEBP. Matrix Biol. 40, 10–16. https://doi.org/10.1016/j.matbio.2014.08.014.

Johnson, Z.I., Shapiro, I.M., Risbud, M.V., 2016. RNA sequencing reveals a role of TonEBP transcription factor in regulation of Pro-inflammatory genes in response to hyperosmolarity in healthy nucleus pulposus cells: a homeostatic response? J. Biol. Chem. 291, 26686–26697. https://doi.org/10.1074/jbc.M116.757732.

José-Edwards, D.S., Kerner, P., Kugler, J.E., Deng, W., Jiang, D., Di Gregorio, A., 2011. The identification of transcription factors expressed in the notochord of Ciona intestinalis adds new potential players to the brachyury gene regulatory network. Dev. Dynam. 240, 1793–1805. https://doi.org/10.1002/dvdy.22656.

Karolchik, D., Hinrichs, A.S., Furey, T.S., Roskin, K.M., Sugnet, C.W., Haussler, D., Kent, W.J., 2004. The UCSC Table Browser data retrieval tool. Nucleic Acids Res. 1 (32), D493–D496. Database issue.

Kent, W.J., Sugnet, C.W., Furey, T.S., Roskin, K.M., Pringle, T.H., Zahler, A.M., Haussler, D., 2002. The human genome browser at UCSC. Genome Res. 12 (6), 996–1006.

Korzh, V., Grunwald, D., 2001. Nadine Dobrovolskaïa-Zavadskaïa and the dawn of developmental genetics. Bioessays 23, 365–371. https://doi.org/10.1002/bies.1052.

López-Rodríguez, C., Antos, C.L., Shelton, J.M., Richardson, J.A., Lin, F., Novobrantseva, T.I., Bronson, R.T., Igarashi, P., Rao, A., Olson, E.N., 2004. Loss of NFAT5 results in renal atrophy and lack of tonicity-responsive gene expression. Proc. Natl. Acad. Sci. U. S. A. 101, 2392–2397.

López-Rodríguez, C., Aramburu, J., Jin, L., Rakeman, A.S., Michino, M., Rao, A., 2001. Bridging the NFAT and NF-kappaB families: NFAT5 dimerization regulates cytokine gene transcription in response to osmotic stress. Immunity 15, 47–58.

Lopez-Rodríguez, C., Aramburu, J., Rakeman, A.S., Rao, A., 1999. NFAT5, a constitutively nuclear NFAT protein that does not cooperate with Fos and Jun. Proc. Natl. Acad. Sci. U. S. A. 96, 7214–7219.

Lu, Q., Bhattachan, P., Dong, B., 2018. Ascidian notochord elongation. Dev. Biol. https://doi.org/10.1016/j.ydbio.2018.11.009.

Macián, F., López-Rodríguez, C., Rao, A., 2001. Partners in transcription: NFAT and AP-1. Oncogene 20, 2476–2489. https://doi.org/10.1038/sj.onc.1204386.

Miyakawa, H., Woo, S.K., Dahl, S.C., Handler, J.S., Kwon, H.M., 1999. Tonicity-responsive enhancer binding protein, a rel-like protein that stimulates transcription in response to hypertonicity. Proc. Natl. Acad. Sci. U. S. A. 96, 2538–2542.

Peck, S.H., McKee, K.K., Tobias, J.W., Malhotra, N.R., Harfe, B.D., Smith, L.J., 2017. Whole transcriptome analysis of notochord-derived cells during embryonic formation of the nucleus pulposus. Sci. Rep. 7, 10504. https://doi.org/10.1038/s41598-017-10692-5.

Pennimpede, T., Proske, J., König, A., Vidigal, J.A., Morkel, M., Bramsen, J.B., Herrmann, B.G., Wittler, L., 2012. In vivo knockdown of Brachyury results in skeletal defects and urorectal malformations resembling caudal regression syndrome. Dev. Biol. 372, 55–67. https://doi.org/10.1016/j.ydbio.2012.09.003.

Postma, A.V., Alders, M., Sylva, M., Bilardo, C.M., Pajkrt, E., van Rijn, R.R., Schulte-Merker, S., Bulk, S., Stefanovic, S., Ilgun, A., Barnett, P., Mannens, M.M.A.M., Moorman, A.F.M., Oostra, R.J., van Maarle, M.C., 2014. Mutations in the T (brachyury) gene cause a novel syndrome consisting of sacral agenesis, abnormal ossification of the vertebral bodies and a persistent notochordal canal. J. Med. Genet. 51, 90–97. https://doi.org/10.1136/jmedgenet-2013-102001.

Reeves, W.M., Wu, Y., Harder, M.J., Veeman, M.T., 2017. Functional and evolutionary insights from the Ciona notochord transcriptome. Development 144, 3375–3387. https://doi.org/10.1242/dev.156174.

Rigueur, D., Lyons, K.M., 2014. Whole-mount skeletal staining. Methods Mol. Biol. 1130, 113–121. https://doi.org/10.1007/978-1-62703-989-5_9.

Risbud, M.V., Guttapalli, A., Stokes, D.G., Hawkins, D., Danielson, K.G., Schaer, T.P., Albert, T.J., Shapiro, I.M., 2006. Nucleus pulposus cells express HIF-1 alpha under normoxic culture conditions: a metabolic adaptation to the intervertebral disc microenvironment. J. Cell. Biochem. 98, 152–159. https://doi.org/10.1002/jcb.20765.

Risbud, M.V., Schoepflin, Z.R., Mwale, F., Kandel, R.A., Grad, S., Iatridis, J.C., Sakai, D., Hoyland, J.A., 2015. Defining the phenotype of young healthy nucleus pulposus cells: recommendations of the Spine Research Interest Group at the 2014 annual ORS meeting. J. Orthop. Res. 33, 283–293. https://doi.org/10.1002/jor.22789.

Risbud, M.V., Shapiro, I.M., 2011. Notochordal cells in the adult intervertebral disc: new perspective on an old question. Crit. Rev. Eukaryot. Gene Expr. 21, 29–41. https://doi.org/10.1615/CritRevEukarGeneExpr.v21.i1.30.

Sagstad, A., Grotmol, S., Kryvi, H., Krossøy, C., Totland, G.K., Malde, K., Wang, S., Hansen, T., Wargelius, A., 2011. Identification of vimentin- and elastin-like transcripts specifically expressed in developing notochord of Atlantic salmon (Salmo salar L.). Cell Tissue Res. 346, 191–202. https://doi.org/10.1007/s00441-011-1262-y.

Silagi, E.S., Batista, P., Shapiro, I.M., Risbud, M.V., 2018a. Expression of carbonic anhydrase III, a nucleus pulposus phenotypic marker, is hypoxia-responsive and confers Protection from oxidative stress-induced cell death. Sci. Rep. 8, 4856. https://doi.org/10.1038/s41598-018-23196-7.

Silagi, E.S., Shapiro, I.M., Risbud, M.V., 2018b. Glycosaminoglycan synthesis in the nucleus pulposus: dysregulation and the pathogenesis of disc degeneration. Matrix Biol. 368–379. https://doi.org/10.1016/j.matbio.2018.02.025.

Stemple, D.L., 2005. Structure and function of the notochord: an essential organ for chordate development. Development 132, 2503–2512. https://doi.org/10.1242/dev.01812.

Stott, D., Kispert, A., Herrmann, B.G., 1993. Rescue of the tail defect of Brachyury mice. Genes Dev. 7, 197–203.

Stroud, J.C., Lopez-Rodriguez, C., Rao, A., Chen, L., 2002. Structure of a TonEBP-DNA complex reveals DNA encircled by a transcription factor. Nat. Struct. Biol. 9, 90–94. https://doi.org/10.1038/nsb749.

Tran, C.M., Markova, D., Smith, H.E., Susarla, B., Ponnappan, R.K., Anderson, D.G., Symes, A., Shapiro, I.M., Risbud, M.V., 2010. Regulation of CCN2/connective tissue growth factor expression in the nucleus pulposus of the intervertebral disc: role of Smad and activator protein 1 signaling. Arthritis Rheum. 62, 1983–1992. https://doi.org/10.1002/art.27445.

Tsai, T.-T., Danielson, K.G., Guttapalli, A., Oguz, E., Albert, T.J., Shapiro, I.M., Risbud, M.V., 2006. TonEBP/OREBP is a regulator of nucleus pulposus cell function and survival in the intervertebral disc. J. Biol. Chem. 281, 25416–25424. https://doi.org/10.1074/jbc.M601969200.

van der Windt, A.E., Haak, E., Das, R.H.J., Kops, N., Welting, T.J.M., Caron, M.M.J., van Til, N.P., Verhaar, J.A.N., Weinans, H., Jahr, H., 2010. Physiological tonicity improves human chondrogenic marker expression through nuclear factor of activated T-cells 5 in vitro. Arthritis Res. Ther. 12, R100. https://doi.org/10.1186/ar3031.

Walmsley, R., 1953. The development and growth of the intervertebral disc. Edinb. Med. J. 60, 341–364.

Wuertz, K., Urban, J.P.G., Klasen, J., Ignatius, A., Wilke, H.J., Claes, L., Neidlinger-Wilke, C., 2007. Influence of extracellular osmolarity and mechanical stimulation on gene expression of intervertebral disc cells. J. Orthop. Res. 25, 1513–1522. https://doi.org/10.1002/jor.20436.